Ray-Density Normalization for Ray-Optical Wave Propagation Modeling in Arbitrarily Shaped Tunnels

Dirk Didascalou, *Student Member, IEEE,* Thomas M. Schäfer, *Student Member, IEEE,* Frank Weinmann, and Werner Wiesbeck, *Fellow, IEEE*

***Abstract*—This work is concerned with the calculation of natural electromagnetic (EM) wave propagation and the determination of the propagation channel characteristics in highway or railway tunnels in the ultrahigh-frequency (UHF) range and above (>300 MHz). A novel ray-tracing technique based on geometrical optics (GO) is presented. Contrary to classical ray tracing, where the one ray representing a locally plane wave front is searched, the new method requires multiple representatives of each physical EM wave at a time. The contribution of each ray to the total field at the receiver is determined by the proposed ray-density normalization (RDN). This technique has the further advantage of overcoming one of the major disadvantages of GO, the failure at caustics. In contrast to existing techniques, the new approach does not use ray tubes or adaptive reception spheres. Consequently, it does not suffer their restrictions to planar geometries. Therefore, it allows to predict the propagation of high-frequency EM waves in confined spaces with curved boundaries, like tunnels, with an adequate precision. The approach is verified theoretically with canonical examples and by various measurements at 120 GHz in scaled tunnel models.**

***Index Terms*—Geometrical optics (GO), measurements, millimeter waves, mobile communications, ray launching, ray tracing, tunnels, wave propagation.**

I. Introduction

THE motto "the freedom to communicate at any time and at any place" implies a complete and seamless coverage for the offered services. Although in mobile communications over land and in urban areas this is mainly achieved, the one Achilles heel is propagation in tunnels. To plan and provide efficient mobile services in tunnels, knowledge of the transmission channel properties is obviously required.

This work is concerned with the calculation of natural electromagnetic (EM) wave propagation and the determination of the propagation channel characteristics in highway or railway tunnels in the UHF frequency range and above (>300 MHz). Realistic tunnel geometries are generally of rectangular cross section or arched shape, i.e., of elliptical cross section with a raised floor and, eventually, an additional ceiling. Furthermore, they are mostly curved [1]. Real-curved or arched-shaped tunnels have only been described in an empirical way based on measurements [2], [3] or by approximate solutions based on modal theory [4]–[6]. Recently, several ray-based methods have been proposed to model the EM wave propagation in tunnels. Irrespective of their ray-tracing technique (ray launching [7], imaging [8]–[11], or a combination of both [12], [13]), they all have in common that they can only treat reflections at plane boundaries. As a consequence, either they only look at rectangular (piecewise) straight tunnel sections [7], [10], [11], or they tessellate more complex geometries into multiple plane facets [13], [14].

In contrast, a novel ray-optical method is presented in this work, which is *not* restricted to plane surfaces. For the first time, it allows a sufficiently accurate ray-tracing-based coherent calculation of the EM field in tunnels of arbitrary shape. The modeling is based on geometrical optics (GO) [15]. Contrary to classical ray tracing, where the one ray representing a locally plane wave front is searched, the new method requires multiple representatives of each physical EM wave at a time. The contribution of each ray to the total field at the receiver is determined by the proposed ray-density normalization (RDN). This technique has the further advantage of overcoming one of the major disadvantages of geometrical optics, the failure at caustics. An important prerequisite of the new method is a dense equal spatial distribution of the traced rays, which is accomplished by a Monte Carlo ray launching. If analytically describable boundaries, like sections of elliptical tori, etc., are used to describe the geometry of the tunnel, the modeling becomes reasonably fast. Additionally, wide-band channel signatures like the power delay profile or parameters, like the delay and Doppler spread, are predicted. The model also handles moving vehicles inside tunnels so that sets of time series can be generated automatically. These sets can for example be used to evaluate the performance of different transmission schemes. The approach is verified theoretically with canonical examples and by various measurements at 120 GHz in scaled tunnel models.

II. Ray Launching and Reception Spheres

The employed ray-optical method is based on ray launching. In ray launching, also referred to as the shooting and bouncing ray (SBR) method [16], a large number of rays is sent out from the transmitter in arbitrary directions. The initial phasors of the rays are determined by the radiation pattern of the transmitting antenna including phase and polarization. Each ray is traced in space and wave propagation is calculated according to GO, including reflection, scattering, etc. [15], [17], [18]. The trace terminates if a ray eventually hits a receiver or when it surpasses a certain maximum attenuation. At the receiver, all incoming

Manuscript received September 21, 1999; revised June 8, 2000.

D. Didascalou, T. M. Schäfer, and W. Wiesbeck are with Institut für Höchstfrequenztechnik und Elektronik (IHE), Universität Karlsruhe (TH), 76128 Karlsruhe, Germany (e-mail: Dirk.Didascalou@etec.uni-karlsruhe.de).

F. Weinmann is with the Institut für Industrielle Informationstechnik (IIIT), Universität Karlsruhe (TH), 76187 Karlsruhe, Germany (e-mail: weinmann@iiit.etec.uni-karlsruhe.de).

Publisher Item Identifier S 0018-926X(00)09363-7.

rays are combined in order to determine the overall reception level. Generally, only a few of the launched rays of which the trajectories have been searched actually hit the receiver. Therefore, ray launching is referred to as an indirect ray-tracing approach. To ensure that all relevant propagation paths are found in the process of ray launching, a sufficiently large number of rays has to be sent out at the transmitter. The major advantage of ray launching is its applicability even in curved geometries. However, the decision, whether a ray hits a receiver or not, is actually one of the most severe problems in ray launching. The two known methods to solve this problem—at least in planar geometry—are discrete ray tubes [19], [20] or reception spheres [21], [22]. Although discrete ray tubes perform well in urban or indoor environments, which are constituted by plane surfaces, they fail at curved geometries. This is because the delimitation of adjacent ray tubes becomes ambiguous after reflection from a curved surface. Therefore, only reception spheres are considered in the following.

For the approach using reception spheres, the receivers are assigned to a certain volume in space, typically a sphere, yielding the termination reception sphere. A launched ray reaches a receiver, if it intersects the corresponding reception sphere. The difficulty with the classical approach of reception spheres is the determination of their size. If the size is too small, only a few rays reach the receiver and the results are inaccurate since important propagation paths may not be considered. On the other hand, if the size is too large, several physically "identical rays" reach the receiver so that the results become faulty without a correct normalization. This *multiple ray problem* is illustrated in Fig. 1, where receiver Rx_1 is reached by multiple direct rays, each representing a distinct wavefront. In reality, however, there is only one physical wavefront reaching the receiver on the direct propagation path and, thus, only one direct ray should be received. The multiple rays can also be classified as being too close to be considered as independent [17].

Additionally, Fig. 1 shows that the number of registered rays also depends on the distance from the transmitter, assuming a constant size of the reception spheres. An approximate solution to overcome those problems in planar geometries are adaptive reception spheres, where the radius of the spheres is proportional to the path length and the angular spacing of the rays at the transmitter [21], [22].

III. Concept of Ray-Density Normalization (RDN) in Curved Geometry

A. The General Approach

If reception spheres are used, a normalization can be found being also valid in curved geometries—contrary to the hitherto usual approach addressed in the previous section. The new concept of RDN is as follows. Instead of trying to avoid the existence of multiple rays, it is *a priori* assumed that several multiple (or dependent) rays are present on each physical propagation path. The number of these rays is determined and this number is used to normalize the contribution of each ray to the total field. As a consequence, the new method requires multiple representatives of each physical EM wave at a time. This is opposed to classical ray tracing, where the one ray representing a locally plane wavefront is searched.

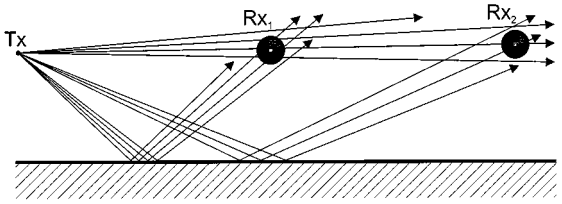

Fig. 1. The multiple ray problem using reception spheres with constant size in ray launching.

B. The Ray Density

In order to determine the number of rays, which reach the receiver on the same propagation path, the ray density is used. The ray density is defined as the number of rays per unit area. In addition to its amplitude, phase, polarization, etc., each ray carries the ray density along its path. If a ray hits a reception sphere, the theoretical number of multiple rays hitting the same sphere can be calculated by simply multiplying the ray density with the area of the sphere.

For a number of N launched, equally distributed, discrete rays in space and the restriction to plane surfaces, the ray density n_d at a distance[1] r from the transmitter is given by

$$n_d = \frac{N}{4\pi r^2}. \tag{1}$$

If reflections at curved surfaces are considered, the proportionality of n_d to $1/r^2$ is no longer valid in general. At curved surfaces the rays can be focused or defocused. It is, e.g., possible that after a reflection at a parabolic reflector the rays are parallel, i.e., n_d becomes independent of r (plane wave). The determination of the ray density n_d in curved geometries is performed according to GO in analogy to the calculation of the electric field after reflection from a curved surface. However, the ray density n_d is not proportional to the electric field $\vec{E}$, but to the radiation density S of a ray. Since $n_d \propto S \propto |\vec{E}|^2$, the ray density can be calculated using the well-established GO formalisms of reflected astigmatig pencil beams [15], [17], [18], [23]. Substituting $|\vec{E}|^2$ in [15, eq. (13-9)], by n_d directly leads to the reflected ray density at a distance s from a curved surface

$$n_d^r(s) = \left| \frac{\rho_1^r \rho_2^r}{(\rho_1^r + s)(\rho_2^r + s)} \right| n_d^i. \tag{2}$$

In (2), n_d^i denotes the incident ray density just before the reflection, $n_d^r(s)$ is the ray density after reflection at a distance s from the point of reflection and $\rho_{1,2}^r$ denote the radii of curvature of the wave front after reflection at $s = 0$. The determination of the radii of curvature ρ^r of the reflected paraxial rays is intensively treated in [15], [17], [18], [23]. The ray density $n_{d,1}^i$ before the first reflection at a curved surface is given by (1). Using (1) and

[1]For example, the unfolded path length normalized to 1 m.

(2), it is now possible to determine the ray density of all rays along their propagation path in any geometry.

C. Determination of the Number of Multiple Rays

If a ray hits the receiver, the theoretical total number M of rays reaching the receiver on the same propagation path is now calculated using the area A of the receiver normal to the propagation direction of the ray, i.e.,

$$M = n_d A. \tag{3}$$

Again, these *multiple rays* are physically identical, i.e., they arrive from the same direction, they have the same delay, number of reflections, etc. Hence, these rays have to be weighted, such that the ensemble of M multiple rays leads to the same result as if only (exactly) one ray would reach the receiver. The weighting thereby depends on the type of analysis, as will be described in Section IV.

D. Prerequisites of the RDN

Prerequisites of the RDN are a large number of rays and their homogeneous distribution in space. The large number requirement results from the discretization in the computer: the theoretical number of multiple rays M given by (3) is a real-valued number. However, the number of actual registered rays is an integer. Consequently, in order to keep the error introduced by the weighting as small as possible, the number of multiple rays has to be sufficiently large. In order to fulfill the first requirement with tolerable computational complexity, all ray-tracing calculations, especially all intersection routines, should be solvable analytically [18]. The second requirement directly results from (3): the relation is only valid for a homogeneous distribution of the rays. This distribution can be achieved by a stochastic generation of the ray directions (Monte Carlo method [18]).

IV. Application of the Ray-Density Normalization

In general, a large number of rays reach the receiver on different propagation paths and interfere, especially in confined spaces as tunnels. The overall field at the receiver is, therefore, given by the complex vector sum of all individual ray contributions. This coherent summation requires a perfect knowledge of the amplitude and phase of each single multipath component. However, already small variations in the geometry of the propagation environment on the order of half the wavelength, like the dimension of a tunnel's cross section or a receiver location, generally lead to a significant change in the phase of each multipath component.[2] Therefore, it is often useful to average the received power over a certain range. This averaging can be easily approximated by using a power sum (or incoherent summation) [18], [24]. The power sum equals the averaged received power, if the phases of the multipath components are completely uncorrelated and if the amplitudes are constant.

In the remainder of this paper, only the ratios of received values (index R) to a reference value (index 0) are examined, whereby absolute values become obsolete. Directly at the transmitter ($r = 0$ m) the ratio cannot be determined since the electric field—and, consequently, the received power—theoretically become infinite [15]. Without loss of generality, suppose that a reference distance $r_0 = 1$ m is assumed, i.e.,

$$\frac{P_R(r_0 = 1\text{ m})}{P_0} = \frac{V_R(r_0 = 1\text{ m})}{V_0} = 1 \tag{4}$$

where the notation $V = |\underline{V}|$ is used for the magnitude of the induced voltage at the output port/terminals of the receiving antenna, and P_R denotes the received power delivered to the load.

[2]Whereas the amplitude remains almost constant.

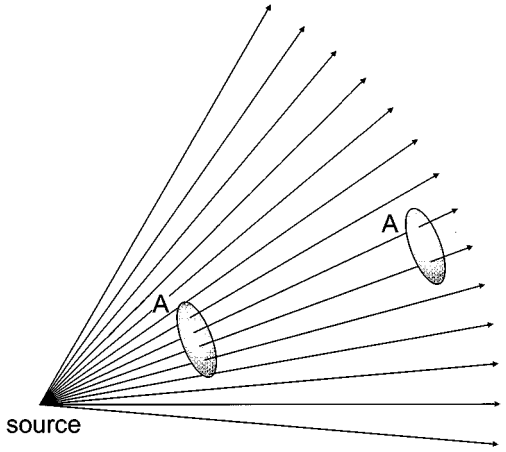

Fig. 2. Geometrical divergence of the power trace approach: at increased distance less rays reach the area A.

A. Relationship Between Divergence of a Ray and Ray Density

Let the loss along a propagation path due to reflection, absorption, etc., be represented by the propagation transfer factor T_P, which also includes the influence of the antennas directivities [18], [23], [24]. The attenuation due to the divergence of the paraxial rays can be represented by the divergence transfer factor T_D. Thus the normalized induced voltage at the receiver for a single physical propagation path or ray is given by

$$\frac{V_R}{V_0} = T_P T_D. \tag{5}$$

For exclusively planar boundaries, the divergence factor is given by $T_D = 1/r$, where r denotes the unfolded pathlength normalized to 1 m. However, at curved boundaries, the radii of curvature of the astigmatic tube of rays have to be considered by taking the ray density of the ideal isotropic source (1) as start density and by cascading (2) accordingly. In this way, the following relation can be established:

$$T_D = \sqrt{\frac{4\pi}{N} n_d}. \tag{6}$$

Now it is possible to state the normalized induced voltage at the receiver in dependence of the ray density

$$\frac{V_R}{V_0} = T_P \sqrt{\frac{4\pi}{N} n_d}. \tag{7}$$

The relative received power results from the square of (7), i.e.,

$$\frac{P_R}{P_0} = \left(\frac{V_R}{V_0}\right)^2 = T_P^2 \frac{4\pi}{N} n_d. \tag{8}$$

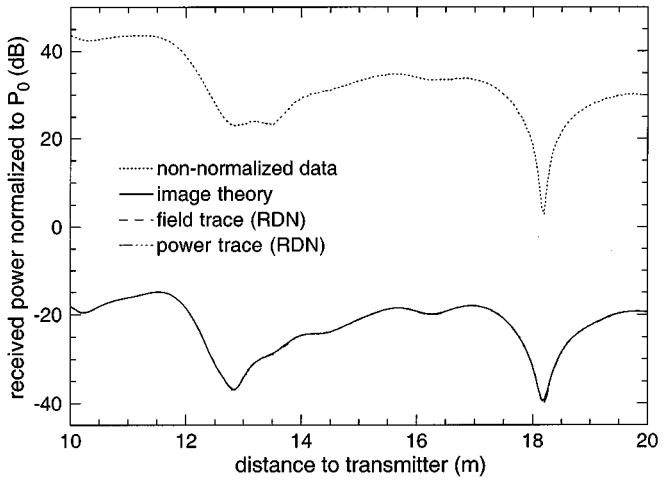

Fig. 3. Coherent comparison of the different approaches in a rectangular waveguide made of dielectric boundaries with $\varepsilon_r = 5$. Distance to vertically polarized isotropic transmitter 10–20 m, 201 receiver points, $f = 1$ GHz, cross section 4 m $\times$ 4 m nonsymmetric arrangement.

In the following sections is shown how the RDN is applied to two different calculation schemes: the so-called field and power traces.

B. Field Trace

The classical approach in ray launching/tracing is to assign a certain electric field strength to each ray, which is normalized to a reference level, as indicated above. The rays are traced until they eventually hit a receiver or until they surpass a certain maximum attenuation. This approach is referred to as *field trace*.

In order to correctly weight the contribution of each ray to the overall received power or the induced voltage at the receiver, weighting factors $X_F^{c/i}$ are introduced. This is because the number of rays reaching the receiver on the same physical propagation path is *a priori* unknown (cf. Section III.A). Furthermore, one has to differentiate if the analysis of multipath propagation is of coherent or incoherent nature. For the coherent analysis, the weighting takes the form

$$V_R^c = V_R X_F^c \tag{9}$$

for the incoherent analysis, the weighting becomes

$$V_R^i = V_R X_F^i. \tag{10}$$

The following considerations are only valid for a single physical propagation path on which several discrete rays with identical amplitude $\underline{V}_R$ reach the receiver. The number of multiple rays is theoretically given by M. The coherent summation of all rays belonging to the same propagation path leads to

$$\frac{P_R^c}{P_0} = \left| \sum_{k=1}^{M} \frac{\underline{V}_{R,k}^c}{V_0} \right|^2 = \left(M \frac{V_R^c}{V_0} \right)^2 = M^2 T_P^2 \frac{4\pi}{N} n_d {X_F^c}^2 \tag{11}$$

which has to match the result of (8), yielding

$$X_F^c = \frac{1}{M} = \frac{1}{n_d A}. \tag{12}$$

The incoherent summation leads to

$$\frac{P_R^i}{P_0} = \sum_{k=1}^{M} \left| \frac{\underline{V}_{R,k}^i}{V_0} \right|^2 = M \left(\frac{V_R^i}{V_0} \right)^2 = M T_P^2 \frac{4\pi}{N} n_d {X_F^i}^2. \tag{13}$$

Comparing the result to (8) gives

$$X_F^i = \frac{1}{\sqrt{M}} = \frac{1}{\sqrt{n_d A}} = X_F^c \sqrt{n_d A}. \tag{14}$$

With (12) and (14), the RDN-based weighting factors are known by which the predicted values of the discrete rays have to be normalized at the receiver in order to obtain valid results.

C. Power Trace

The idea of the *power trace* is to look at the power (respectively, energy) of each ray instead of the habitual electric field. This method is the standard approach in ray tracing for computer graphics [25]. The total radiated power of the transmitter is spread over all rays. Each ray "keeps" its portion of the power on its way through the tunnel, attenuation may occur due to propagation phenomena like reflection, etc. If a ray hits a receiver, it is assumed that its remaining power is transferred totally to the receiver. The summation over all received rays gives the received total power. Focusing effects for instance may occur, if a huge number of rays hit the receiver. On the other hand, the effect of free-space attenuation is included implicitly: at increased distance, less rays, and, thus, less power reach the receiver due to geometrical divergence (cf. Fig. 2). In contrast to the field trace, where each ray represents a locally plane wave and, therefore, can be treated separately, only the ensemble of all rays reaching the receiver makes sense in physical terms for the power trace.

The initial power P_t of each ray is determined by the input power P_T, the transmitting antenna characterized by G_T (gain) and $\underline{\vec{C}}_T$ (directional antenna pattern) and the number of launched rays N, yielding

$$P_t = \frac{P_T G_T |\underline{\vec{C}}_T|^2}{N}. \tag{15}$$

If no propagation losses occur, the assumption that a ray delivers its total energy to the receiver can be expressed by

$$S_A = \frac{P_t}{A}. \tag{16}$$

Here A denotes the area of the receiver and S_A the radiation density, which the ray tube (corresponding to the discrete ray) would have, if its area equalled A. The approximation is valid for

$$A_{\mathrm{rt}} \leq A \approx A_{eR} = \frac{\lambda_0^2}{4\pi} G_R \tag{17}$$

where

- A_{rt} actual area of the ray tube;
- A_{eR} effective area of the receiving antenna;
- λ_0 free-space wavelength;
- G_R gain of the receiving antenna.

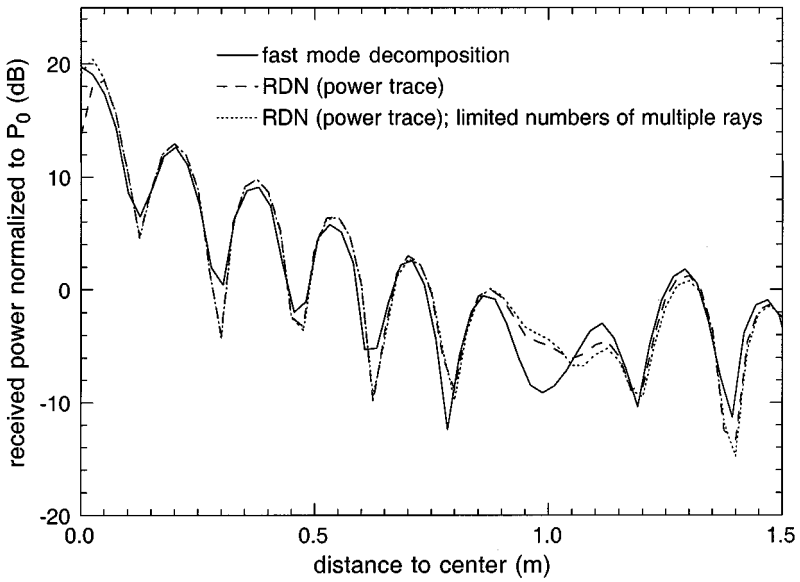

Fig. 4. Comparison of RDN and mode decomposition in an ideal metallic corrugated circular waveguide from center to outer wall, distance to transmitter 10 m, radius of the waveguide 2 m, 80 receiver points, centric position of isotropic transmitter, $f = 1$ GHz.

The contribution of the ray to the total received power is obtained using A_{eR}, leading to

$$P_R = S_A A_{eR} = \frac{P_t}{A} A_{eR} = \frac{\lambda_0^2}{4\pi AN} P_T G_T G_R T_P^2. \quad (18)$$

To overcome the loss-free requirement of (16), the propagation transfer factor T_P is necessary in the previous equation to account for the dissipation of energy[3] on the propagation path due to the different propagation phenomena. However, no divergence factor is introduced since the power of the ray is regarded, not its radiation density. Equation (18) points out that only the ensemble of all received rays has a physical meaning. This can easily be verified for the free-space case with $T_P = 1$. The area of the receiver A at a distance r to the source is reached by

$$M = \frac{AN}{4\pi r^2} \quad (19)$$

rays, assuming N rays equally distributed over the solid angle 4π (cf. Fig. 2). This results in a total received power of

$$P_{R,\mathrm{tot}} = \sum_{k=1}^{M} P_{R,k} = MP_R = \left(\frac{\lambda_0}{4\pi r}\right)^2 P_T G_T G_R \quad (20)$$

which equals the Friis transmission equation [26].

For the general case—including reflection, etc., the same approach as in the previous section is adopted. First, the power of each single ray is normalized leading to

$$\frac{P_R}{P_0} = T_P^2 \quad (21)$$

or equivalently

$$\frac{V_R}{V_0} = T_P. \quad (22)$$

[3] T_P also includes the influence of the antenna directivities (cf. Section IV-A).

The phase of the induced voltage at the receiver is determined by the traversed path length and phase jumps of $+90°$ at potential passages through caustics [15], [16]. However, (22) only states the contribution of a single ray. Again, the number of rays arriving at the receiver on the same physical propagation path is *a priori* unknown. Therefore, according to the field trace case, weighting factors are introduced that are based on the RDN. Finally, the actual value at the receiver is achieved by weighting and superposition of all incoming rays. In an analogy to Section IV-B, the coherent summation is in the form

$$\frac{P_R^c}{P_0} = \left|\sum_{k=1}^{M} \frac{V_{R,k}^c}{V_0}\right|^2 = \left(M\frac{V_R^c}{V_0}\right)^2 = M^2 T_P^2 {X_P^c}^2 \quad (23)$$

yielding

$$X_P^c = \sqrt{\frac{4\pi}{N}\frac{n_d}{M^2}} = \sqrt{\frac{4\pi}{N}\frac{1}{n_d A^2}} = \sqrt{\frac{4\pi}{NA}\frac{1}{M}} \quad (24)$$

after comparison with (8). The power sum, on the other hand, is given by

$$\frac{P_R^i}{P_0} = \sum_{k=1}^{M} \left|\frac{V_{R,k}^i}{V_0}\right|^2 = M\left(\frac{V_R^i}{V_0}\right)^2 = MT_P^2 {X_P^i}^2 \quad (25)$$

leading to

$$X_P^i = \sqrt{\frac{4\pi}{NA}} = X_P^c \sqrt{n_d A}. \quad (26)$$

For both the field and the power trace, the following relation holds:

$$X^i = X^c \sqrt{n_d A} \quad (27)$$

i.e., (27) is independent of the approach.

Because of the introduced factors, the actual computation of the coherent results is essentially the same for both the field and the power trace. Only the way these methods are derived differs: the conventional straight forward analytical formalism for the field trace and the more graphical approach for the power trace. The difference between the two methods, however, becomes significant for the incoherent analysis. The incoherent weighting factor X_P^i of the power trace is constant according to (26) and, therefore, independent of the ray density. This means, the complicated and time-consuming calculation of the ray density can be omitted speeding up the simulation considerably if only the power sum is of interest in the analysis [27].

Furthermore, the power trace in combination with the RDN allows overcoming one of the major disadvantages of GO: its failure at caustics. In a caustic, the predicted GO field—and, therefore, the received power—approach infinity [15]. For the power trace approach, however, the received power is determined by the number of rays, which actually reach the receiver. This number is always finite and smaller than the number of launched rays N. Consequently, even if all rays reached the receiver, the maximum received power would always be lower than (or equal to) the input power of the transmitting antenna P_T in the incoherent analysis. The only variable, which reflects the GO behavior, is the ray density n_d needed for the weighting in the coherent analysis. In (24), the ray density n_d is used together with the visible area of the receiver A to determine the theoretical number of multiple received rays $M = n_d A$. In a caustic, this value would approach infinity. Heuristically, it can now be bound by the maximum value of N or by a fraction of it.

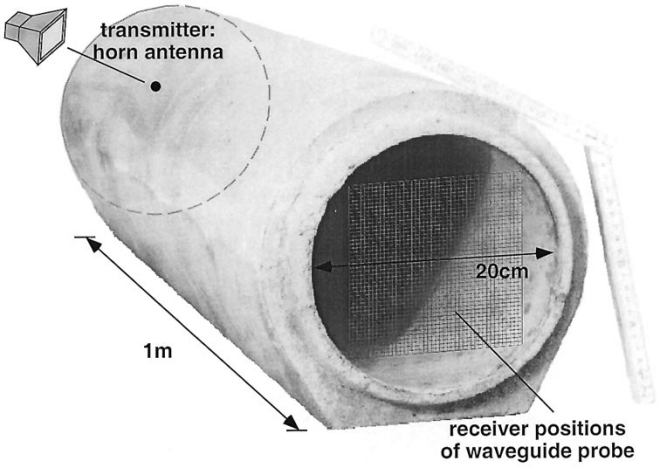

Fig. 5. Measurement setup with a concrete tube; diameter: 20 cm, length: 1 m, $\varepsilon_r \approx 5$, transmitter: horn antenna at tunnel entrance, receiver: waveguide probe for 2-D cross-sectional scans at tunnel exit (resolution: 2 mm × 2 mm), $f = 120$ GHz.

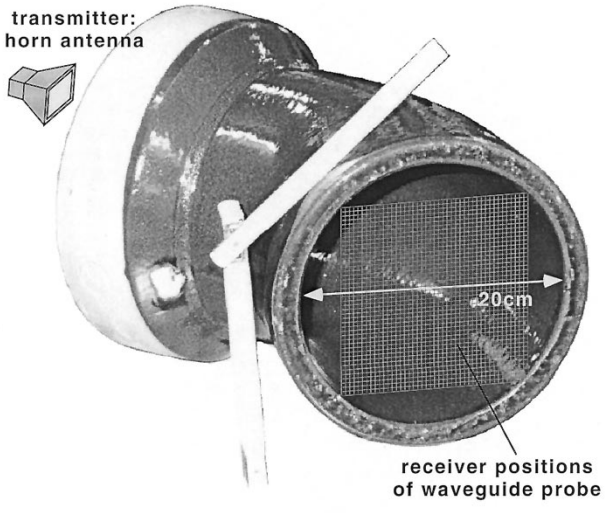

Fig. 6. Measurement setup with a bent stoneware tube; angle of curvature: 45°, diameter: 20 cm, length: 30 cm, $\varepsilon_r \approx 8$, transmitter: horn antenna at tunnel entrance, receiver: waveguide probe for 2-D cross-sectional scans at tunnel exit (resolution: 2 mm × 2 mm), $f = 120$ GHz.

V. Verification

In this section, the proposed modeling approach is compared to theoretical "reference solutions" in canonical geometries, followed by comparisons with measurements at 120 GHz in scaled model tunnels.

A. Theoretical Validation

1) Rectangular Waveguide: First, comparisons are made in a rectangular waveguide with dielectric boundaries using image theory as ray-optical reference [9]–[11], [28]. The dimensions of the cross section are 4 m × 4 m, the walls have a permittivity of $\epsilon_r = 5$. The isotropic transmitter is situated at the entrance of the waveguide, 1.1 m from the left wall and 2.1 m above ground. The receivers have a variable distance to the transmitter, 1.9 m from the left wall and 1.7 m above ground. The carrier frequency is $f = 1$ GHz. The scenario is chosen to avoid any symmetry effects [13]. Except for image theory 20 million rays are launched equally distributed in space by a stochastic ray launching and up to ten reflections are included, ensuring sufficient convergence of the results. Fig. 3 depicts the coherent comparison of the reference solution, the field and the power trace with RDN, and the uncorrected "raw" ray launching. Obviously, the nonnormalized curve does not fit the reference solution. Apart from the very high predicted level, it generally decreases too fast with distance, indicating a nonconstant offset. At increased distances, less rays reach the receiver resulting in a decreasing total received power level. On the other hand, the two RDN-based approaches match the image theory results very well. The computation time of the RDN-based methods was 1:30 h on a Hewlett Packard C-series workstation with 240-MHz clock rate.

To allow for curved boundaries, an ideal corrugated circular waveguide is considered in the next section.

2) Corrugated Circular Waveguide: In the previous section, it was shown that the proposed RDN-based methods work well in a rectangular shaped straight tunnel. Unfortunately, in tunnels of curved cross section no ray-optical reference solution like image theory is available. This is because an unambiguous image of a point only exists at planar surfaces. Thus, another strategy for validation has been chosen. First, the two RDN-based models are compared. It comes out that both field and

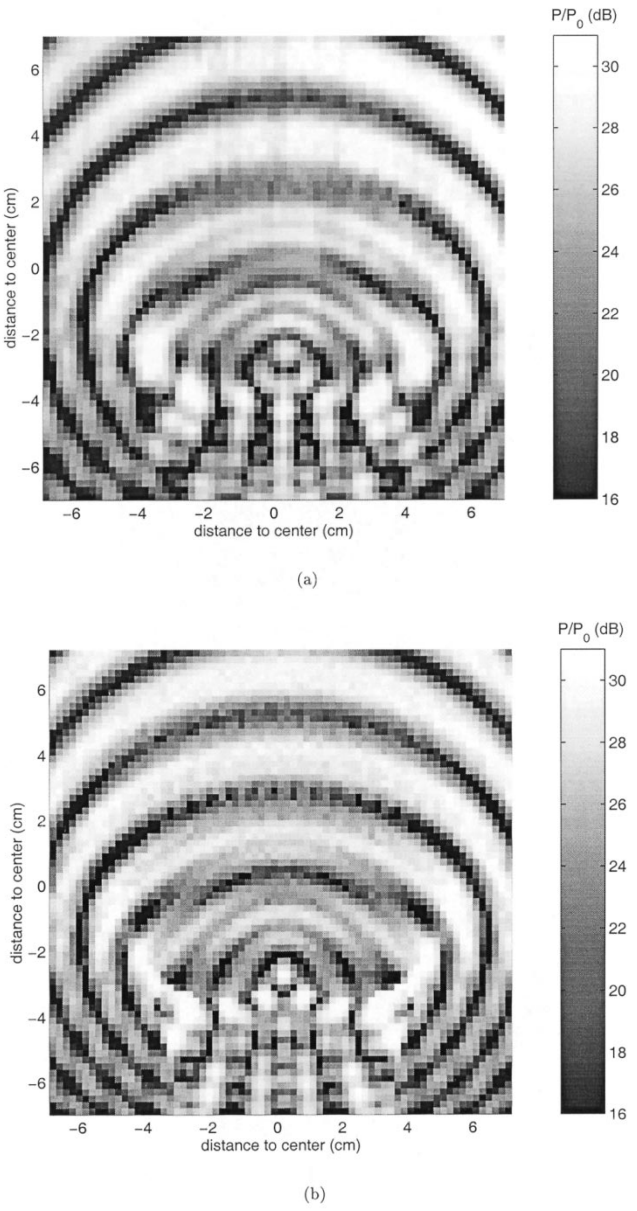

Fig. 7. Results for measurement setup according to Fig. 5, transmitter 5 cm above center, scanned area: 71 × 71 points, resolution: 2 mm (coherent analysis, vv-polarization). (a) Measurement at 120 GHz. (b) Simulation at 120 GHz.

power trace deliver the same results in curved geometry, wherefore in the following, only the results of the power trace are stated.

For the theoretical verification, a fictitious ideal metallic corrugated circular waveguide is assumed. An ideal corrugated waveguide is a special waveguide with Fresnel reflection coefficients $R_{||} = R_{\perp} = -1$. This behavior is achieved by a special geometry of grooves on the inner surface of the waveguide, also named corrugation [29]. In practice, corrugated waveguides are, e.g., used in microwave technology for power transmission or dish antenna feed systems. The reference solution utilized in this geometry is based on fast mode decomposition [30]. The field is decomposed in modes, where only the propagating modes are considered.

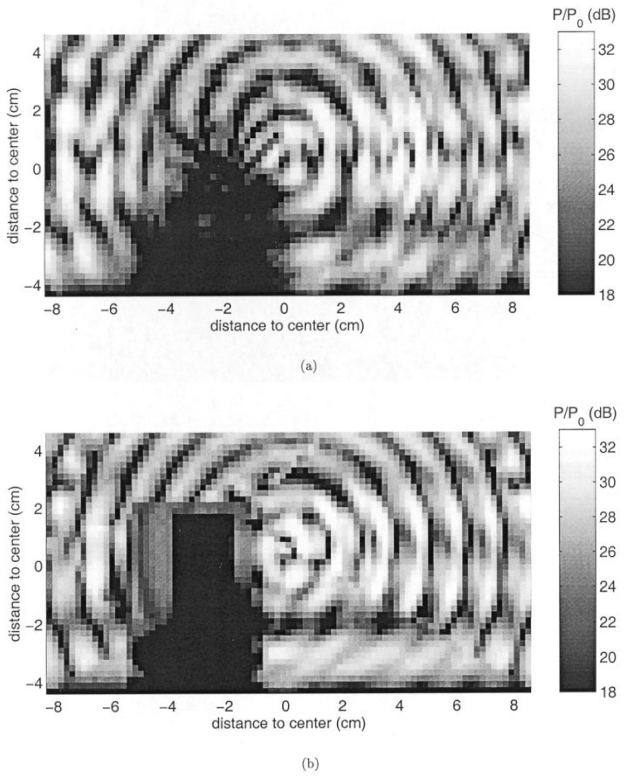

Fig. 8. Results for measurement setup according to Fig. 5 with PVC-floor ($\epsilon_r \approx 2.5$) and box-like vehicle, centric transmitter position, scanned area: 81 × 46 points, resolution: 2 mm (coherent analysis, vv-polarization). (a) Measurement at 120 GHz. (b) Simulation at 120 GHz.

Fig. 4 shows the comparison of the analytical method and the RDN-based power trace in a waveguide with radius 2 m at $f = 1$ GHz. An ideal isotropic transmitter is placed in the center of the waveguide, the receivers are situated along the line center-to-outer-wall at 10 m from the transmitter. For the RDN-based power trace, two different curves are plotted in Fig. 4: one with the weighting factors given by (24); the other is bound to a maximum number of multiple rays $M_{\max} = N/1000$ in order to predict correct values near caustics (cf. Section IV-C). Taking into account the ideal lossless surface of the corrugated waveguide, even rays with a high number of reflections are still contributing to the overall reception level. Therefore, sufficient convergence of the ray tracing is only possible with considerable computational effort. For the simulation in Fig. 4 200 million rays have been traced with up to 200 reflections. The simulation time on a Hewlett Packard C-series workstation with 240-MHz clock rate was about one day. Despite the critical circumstances of ideal lossless surfaces, which represent a numerical worst-case scenario in ray launching, a very good agreement of the results is observed. This validates the developed new RDN, as well as the implementation of ray tracing.

B. Verification by Measurements

In the previous chapter the proposed RDN has been validated theoretically. This was only possible in idealized geometries for which reference solutions exist. To test the RDN in realistic geometry, measurements have been carried out at 120

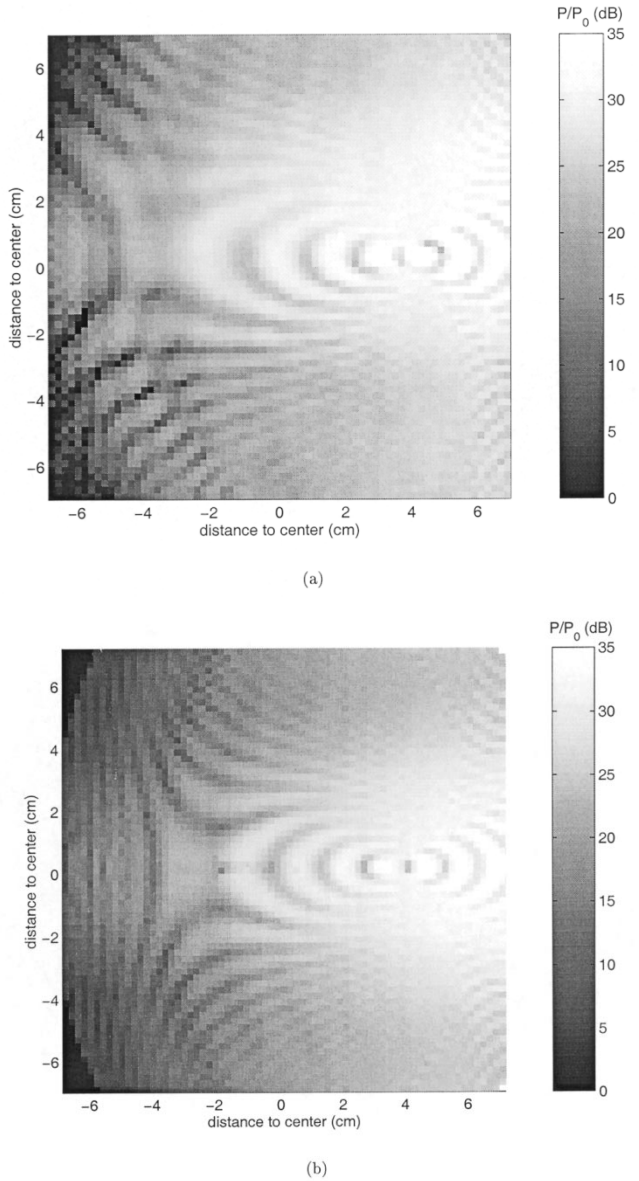

Fig. 9. Results for measurement setup according to Fig. 6, transmitter in eccentric position 5 cm from the center in the direction of the bend, scanned area: 71 × 71 points, resolution: 2 mm (coherent analysis, vv-polarization). (a) Measurement at 120 GHz. (b) Simulation at 120 GHz.

GHz in scaled model tunnels built of concrete and stoneware. The performance of the modeling approach in real three-dimensional curvature is therefore of primary interest. The frequency of $f = 120$ GHz in the scaled geometry is comparable to a frequency of 1–3 GHz in real tunnels.

1) Measurement Setup and Procedure: Figs. 5 and 6 show the two measurement setups: a straight concrete tube with length of 1 m and diameter of 20 cm (Fig. 5), and a bent stoneware tube with angle of curvature of 45°, length of 30 cm, and diameter of 20 cm (Fig. 6) are used as model tunnels. A standard gain pyramidal D-band (110–170 GHz) horn antenna is used as transmitter at $f = 120$ GHz. The input power of the antenna $P_T \approx 10$ dBm is generated by a backward wave oscillator (BWO). The receiver is a D-band rectangular waveguide probe, which can be displaced computer controlled to generate two-dimensional (2-D) scans with a resolution of 2 mm × 2 mm. The received power level is measured with a vector network analyzer (VNWA). The measurement equipment was developed at the Institut für Hochleistungsimpuls und Mikrowellentechnik, Forschungszentrum Karlsruhe, Karlsruhe, Germany [31], [32]. To avoid noticeable side effects by the edges of the tubes, the transmitter as well as the waveguide probe are positioned at least 1 cm inside the tubes. Despite the tolerances in the geometry of the different tubes and the extremely small wavelengths ($\lambda = 2.5$ mm) a coherent analysis is chosen for comparison purposes in the following section.

2) Comparisons of Measurements and Simulations: For simulation work 50, respectively, 100 million rays are traced with up to ten reflections. The permittivity of the concrete tube is $\epsilon_r = 5$, the one of the stoneware bend is $\epsilon_r = 8$. The surface roughness of the tubes is $\sigma \leq 0.1$ mm. The measured directional pattern of the horn antenna is considered in the simulations. The simulation times are between one and four hours on a HP C-Series Workstation with 240-MHz clock rate.

First, the straight concrete tube of Fig. 5 is examined. Fig. 7 shows the measured and simulated power-level distribution (coherent analysis, vv-polarization) at the end of the tube for an eccentric transmitter position 5 cm above the center at the tunnel entrance. The measurement and the simulation results agree very well. Only in the lower regions of the figures small discrepancies occur, which may be due to a small misalignment of the antennas.

Thereafter, a configuration with a road lane made of PVC $(\varepsilon_r \approx 2.5)$ and a matchbox car ("London Sightseeing Bus") is used. The thickness of the lane is approximately 1 cm. The vehicle resembles a rectangular box (length: 11.7 cm, width: 3.6 cm, height: 6.4 cm, distance between lane and underbody of the car: 0.3 cm) with various windows, whose dimensions are on the order of several wavelengths. The matchbox car is positioned inside the tunnel, 5 cm from the tunnel exit, such that a distinct shadow is visible in the analysis. Although the vehicle is only modeled as a floating PEC rectangular box, the measurement [Fig. 8(a)] and the simulation [Fig. 8(b)] are quite similar. In both figures the circular structures coincide, as well as the horizontal stripes of high (respectively low) reception levels. Also the boundary condition for grazing incidence is visible at the surface of the lane, which calls for a minimum of the received power level.

Finally, the bent stoneware tube of Fig. 6 is used as scaled model tunnel. The transmitter is positioned at the entrance of the tube in an eccentric position 5 cm from the center in the direction of the bend. Fig. 9 depicts the measurement and the simulation at the other end of the tunnel. The great tolerances in the geometry of the bent tube, which is originally intended for the use in sewers, make the comparison quite difficult: the bend is neither circular, nor constant over the whole length. Nevertheless, the simulation [Fig. 9(b)], which assumes piecewise constant and circular bends, and the measurement [Fig. 9(a)] suggest a good agreement over a large area. The influence of the relatively strong bend can be identified by the elliptical structures on the right side of the pictures. A simulation of the same scenario but without bend leads to a concentration of the energy on the other (left) side without the elliptical structures.

The qualitative comparisons of this section reveal the power of the proposed GO-based RDN: all relevant effects in straight tunnels, curved tunnels, and tunnels with vehicles are predicted very well in agreement to measurements.

VI. Conclusion

A novel stochastic ray launching with RDN is presented, which allows the prediction of the signal level in curved geometries like tunnels of different cross sections and shape. An important prerequisite of the approach is a large number of traced rays, which are homogeneously distributed in space. This can easily be reached in confined spaces like tunnels, where all rays are always reflected back into the tunnel area, and the lengths of the propagation paths are limited, resulting in a sufficiently large ray density. Furthermore, if the geometry can be modeled in a way that all intersection problems are solvable analytically, the computation becomes reasonably fast. The normalization is thereby applicable to different ray tracing techniques.

The method is verified theoretically in a waveguide with dielectric boundaries using image theory and in a perfectly conducting corrugated circular waveguide utilizing fast mode decomposition. Several measurements have been conducted at 120 GHz in scaled model tunnels of different shape and course with and without enclosed vehicle. Altogether, the simulation results are validated very well by the measurements. Thus, the proposed modeling approach is applicable for the simulation of high-frequency EM wave propagation in curved tunnels.

Acknowledgment

The authors would like to thank the anonymous reviewers, whose proposed changes increased the value of this paper considerably.

References

[1] A. Straßenentwurf, "Dokumentation für Straßentunneln in Deutschland," Forschungsgesellschaft für Straßen- und Verkehrswesen, Köln, Tech. Rep., 1996. (in German).

[2] J. Chiba, T. Inaba, Y. Kuwamoto, O. Banno, and R. Sato, "Radio communication in tunnels," *IEEE Trans. Microwave Theory Tech.*, vol. MTT-26, pp. 439–443, 1978.

[3] Y. Yamaguchi, T. Abe, and T. Sekiguchi, "Radio wave propagation loss in the VHF to microwave region due to vehicles in tunnels," *Trans. Electromagn. Compat.*, vol. 31, pp. 87–91, Feb. 1989.

[4] S. F. Mahmoud and J. R. Wait, "Guided electromagnetic waves in a curved rectangular mine tunnel," *Radio Sci.*, vol. 9, no. 5, pp. 567–572, 1974.

[5] P. Delogne, "EM propagation in tunnels," *IEEE Trans. Antennas Propagat.*, vol. 39, pp. 401–405, Mar. 1991.

[6] Y. Yamaguchi, T. Abe, T. Sekiguchi, and J. Chiba, "Attenuation constants of UHF radio waves in arched tunnels," *IEEE Trans. Microwave Theory Tech.*, vol. MTT-33, pp. 714–718, 1985.

[7] Y. P. Zhang, Y. Hwang, and R. G. Kouyoumjian, "Ray-optical prediction of radio-wave propagation characteristics in tunnel environments—Part 2: Analysis and measurements," *IEEE Trans. Antennas Propagat.*, vol. 46, pp. 1337–1345, Sept. 1998.

[8] P. Mariage, "Etude théorique et expérimentale de la propagation des ondes hyperfréquences en milieu confiné ou urbain," Ph.D. dissertation, Univ. Lille, France, 1992. (in French).

[9] B. Rembold, "Simulation of radio transmission in a tunnel," *Frequenz*, vol. 47, no. 11/12, pp. 270–275, 1993. (in German).

[10] T. Klemenschits, "Mobile Communications in Tunnels," Ph.D. dissertation, Univ. Wien, Austria, 1993.

[11] P. Mariage, M. Lienard, and P. Degauque, "Theoretical and experimental approach of the propagation of high frequency waves in road tunnels," *IEEE Trans. Antennas Propagat.*, vol. 42, pp. 75–81, Jan. 1994.

[12] S.-H. Chen and S.-K. Jeng, "An SBR/image approach for indoor radio propagation in a corridor," *IEICE Trans. Electron.*, vol. E78-C, no. 8, pp. 1058–1062, 1995.

[13] ——, "SBR image approach for radio wave propagation in tunnels with and without traffic," *IEEE Trans. Veh. Technol.*, vol. 45, pp. 570–578, 1996.

[14] S.-C. Hung, C.-C. Chiu, and C.-H. Chen, "Wireless communication characteristics for tunnels with and without traffic," in *IEEE Int. Conf. Universal Personal Communications (ICUPC'98)*, Florence, Italy, Oct. 1998, pp. 117–122.

[15] C. A. Balanis, *Advanced Engineering Electromagnetics*. New York: Wiley, 1989.

[16] H. Ling, R.-C. Chou, and S.-W. Lee, "Shooting and bouncing rays: Calculating the RCS of an arbitrarily shaped cavity," *IEEE Trans. Antennas Propagat.*, vol. 37, pp. 194–205, Feb. 1989.

[17] G. A. Deschamps, "Ray techniques in electromagnetics," *Proc. IEEE*, vol. 60, pp. 1022–1035, Sept. 1972.

[18] D. Didascalou, "Ray-optical wave propagation modeling in arbitrarily shaped tunnels," Ph.D. dissertation, Univ. Karlsruhe (TH), Germany, 2000, http://www.ubka.uni-karlsruhe.de/cgi-bin/psview?document=2000/elektrotechnik/2.

[19] D. J. Cichon, T. Zwick, and J. Lähteenmäki, "Ray optical indoor modeling in multifloored buildings: Simulations and measurements," in *Proc. IEEE Antennas Propagat. Soc. Int. Symp.*, Newport Beach, CA, June 1995, pp. 522–525.

[20] H. Suzuki and A. S. Mohan, "Ray tube tracing method for predicting indoor channel characteristics map," *Inst. Elect. Eng. Electron. Lett.*, vol. 33, no. 17, pp. 1495–1496, 1997.

[21] W. Honcharenko, H. L. Bertoni, J. L. Dailing, J. Qian, and H. D. Yee, "Mechanisms governing UHF propagation on single floors in modern office buildings," *IEEE Trans. Veh. Technol.*, vol. 41, pp. 496–504, 1992.

[22] S. Y. Seidl and T. S. Rappaport, "Site-specific propagation prediction for wireless in-building personal communication system design," *IEEE Trans. Veh. Technol.*, vol. 43, pp. 879–891, 1994.

[23] G. A. J. van Dooren, "A deterministic approach to the modeling of electromagnetic wave propagation in urban environments," Ph.D. dissertation, Tech. Univ. Eindhoven, The Netherlands, 1994.

[24] N. Geng and W. Wiesbeck, *Planungsmethoden für die Mobilkommunikation, Funknetzplanung unter realen physikalischen Ausbreitungsbedingungen*. Berlin, Germany: Springer-Verlag, 1998. (in German).

[25] A. S. Glassner, Ed., *An Introduction to Ray Tracing*. New York: Academic, 1989.

[26] C. A. Balanis, *Antenna Theory, Analysis and Design*. New York: Wiley, 1997.

[27] J. S. Lamminmäki and J. J. A. Lempiäinen, "Radio propagation characteristics in curved tunnels," *Proc. Inst. Elect. Eng.—Microwaves, Antennas, Propagat.*, vol. 145, no. 4, pp. 327–331, 1998.

[28] S. F. Mahmoud and J. R. Wait, "Geometrical optical approach for electromagnetic wave propagation in rectangular mine tunnels," *Radio Sci.*, vol. 9, no. 12, pp. 1147–1158, 1974.

[29] P.-S. Kildal, "Artificially soft and hard surfaces in electromagnetics," *IEEE Trans. Antennas Propagat.*, vol. 38, pp. 1537–1544, Oct. 1990.

[30] G. Michel and M. Thumm, "Spectral domain techniques for field pattern analysis and synthesis," *Surveys Mathematics Industry: Special Issue Scientific Computing Elect. Engrg.*, vol. 8, pp. 259–270, 1999.

[31] A. Arnold, "Entwicklung eines vektoriellen mm-wellen-netzwerkanalysators mit hoher meßdynamik und messungen an überdimensionierten wellenleiterkomponenten," M.S. thesis, IHE, Univ. Karlsruhe (TH), Germany, 1997. (in German).

[32] O. Schindel, "Entwicklung einer automatisierten meßwerterfassung für einen vektoriellen millimeterwellen-netzwerkanalysator mit hoher dynamik," M.S. thesis, IHE, Univ. Karlsruhe (TH), Germany, 1999. (in German).

Dirk Didascalou (S'96) was born in Hamburg, Germany, in 1969. He received the Dipl. Ing. (M.S.E.E.) and the Dr. Ing. (Ph.D.) degrees in electrical engineering from the Universität Karlsruhe (TH), Karlsruhe, Germany, in 1996 and 2000, respectively.

He took part in the joint Electronic Engineering Degree Scheme within Europe: Paris, Southampton, Karlsruhe (TRIPARTITE). Since 1996, he has been with the Institut für Höchstfrequenztechnik und Elektronik (IHE), Universität Karlsruhe (TH) as a Research Assistant. His research activities are presently focused on millimeter-wave propagation, mobile-to-mobile communications, mobile broad-band links, and wave propagation in tunnels. He is participating as an Expert in the European COST259. He serves as a Lecturer for electromagnetic wave propagation and radio network planning for the Carl Cranz Series for scientific education.

Thomas M. Schäfer (S'99) was born in Karlsruhe, Germany, in 1973. He received the Dipl. Phys. degree in physics from the Universität Karlsruhe (TH), Karlsruhe, Germany, in 1999. He is currently working toward the Dr.-Ing. (Ph.D.) degree in electrical engineering at the Institut für Höchstfrequenztechnik und Elektronik (IHE), Universität Karlsruhe (TH).

His current research interests include millimeter-wave propagation, mobile-to-mobile communications, wave propagation in confined spaces like tunnels, and the investigation of electromagnetic compatibility in hospitals.

Frank Weinmann received the diploma in physics from the Universität Karlsruhe (TH), Karlsruhe, Germany, in 1999. He is currently working toward the Ph.D. degree in electrical engineering at the same university.

In 1999, he joined the Institute of Industrial Information Technology, Universität Karlsruhe (TH). His research interests lie in the field of electromagnetic compatibility of powerline communications.

Werner Wiesbeck (SM'87–F'94) received the Dipl. Ing. (M.S.E.E.) and the Dr. Ing. (Ph.D.E.E.) degrees from the Technical University, Munich, Germany, in 1969 and 1972, respectively.

From 1972 to 1983, he was with AEG-Telefunken in various positions including that of Head of Research and Development of the Microwave Division, Flensburg, Germany, and Marketing Director of the Receiver and Direction Finder Division, Ulm, Germany. During this period, he had product responsibility for millimeter-wave radars, receivers, direction finders, and electronic warfare systems. Since 1983, he has been Director of the Institut für Höchstfrequenztechnik und Elektronik (IHE), Universität Karlsruhe (TH), Germany. His research topics include radar, remote sensing, wave propagation, and antennas. In 1989 and 1994, respectively, he spent a six-month sabbatical at the Jet Propulsion Laboratory, Pasadena, CA. He serves as a permanent Lecturer for radar system engineering and for wave propagation for the Carl Cranz Series for Scientific Education.

Dr. Wiesbeck is President of the IEEE GRS-S (2000–2001), member of the IEEE GRS-S AdCom (1992–2001), past Chairman of the GRS-S Awards Committee (1994–1998), past Executive Vice President IEEE GRS-S (1998–1999), past Associate Editor IEEE TRANSACTIONS ON ANTENNAS AND PROPAGATION (1996–1999), and past Treasurer of the IEEE German Section. He has been General Chairman of the 1988 Heinrich Hertz Centenial Symposium, the 1993 Conference on Microwaves and Optics (MIOP'93). He has been a member of scientific committees of many conferences. He is a member of an Advisory Committee of the EU—Joint Research Centre (Ispra/Italy) and is an advisor to the German Research Council (DFG), to the Federal German Ministry for Research and to industry in Germany.